Growth, Characterization, and Stability Testing of Epitaxial MgO (100) on GaAs (100)

K. Mudiyanselage, M. A. Nadeem, H. A. Raboui, H. Idriss*
Hydrogen Platform, Catalysis Department,
SABIC-Corporate Research and Development (CRD) at KAUST, 23955-Thuwal, Saudi Arabia

Abstract

Epitaxial MgO (100) films have been grown on GaAs (100) by evaporation of Mg in the presence of 5×10^{-6} Torr of oxygen. Prior to the growth of MgO, the GaAs (100) substrate was cleaned by Ar ion sputtering and annealing. MgO (100) on GaAs (100) was in situ characterized with Auger electron spectroscopy (AES), and ex situ by scanning electron microscopy (SEM), X-ray diffraction (XRD), high-resolution transmission electron microscopy (HRTEM), and energy–dispersive X–ray spectroscopy (EDX). X-ray diffraction patterns indicated that the MgO film has grown predominantly in the cubic phase with the (100) plane parallel to the GaAs (100) substrate. HRTEM results have confirmed the epitaxial growth of MgO with MgO (100)[001]‖ GaAs (100)[001]. Despite the high lattice misfit, the epitaxial MgO (100) is grown on GaAs (100) due to the 4 : 3 relationship (4 aMgO : 3 aGaAs) between MgO (100) and GaAs (100). The formation of a 4:3 superstructure reduces the lateral misfit between MgO (100) and GaAs (100) to ≈0.65%. To test the potential of MgO as a protection layer for III-V semiconductor based photo-electro catalytic devices for water splitting in alkaline media the reaction of MgO films with H_2O and NaOH was investigated. Flake-like $Mg(OH)_2$ structures appear to have formed on top of the MgO films treated with NaOH.

Key words

Epitaxial MgO (100) films; GaAs (100); flake-like $Mg(OH)_2$ structures; MgO (100) grown on GaAs (100); lateral misfit between MgO (100) and GaAs (100).

*Corresponding author's Email: idrissh@sabic.com

1. Introduction

Growth of epitaxial MgO thin films on GaAs substrates has received considerable attention, due to unique electronic properties of MgO/GaAs systems [1, 2]. In previous studies, MgO films were grown on GaAs (100) mainly by direct evaporation instead of Mg in the presence of O_2 using different techniques. In some studies, reactive magnetron sputtering was applied to deposit MgO directly on GaAs [3, 4]. Direct deposition of MgO by electron beam evaporation without additional oxygen was also reported previously [1, 5-7]. Lu et al. used an evaporation cell to deposit MgO directly.[8, 9] Electron beam evaporation of MgO in the presence of O_2 was also applied to deposit MgO on GaAs(100)[9]. Nashimoto et al. applied pulsed laser deposition (PLD) method to deposit MgO [10, 11]. In most studies, good epitaxial growth of MgO on GaAs(100) was observed in the temperature range of 400–600 °C, while others reported a polycrystalline MgO morphology with a preferential (100) growth [4] or showed an amorphous MgO intermediate layer at the interface at lower temperatures [12].

Only two studies reported the growth of MgO on GaAs by evaporating pure Mg metal in the presence of oxygen. Pulsed DC magnetron sputtering was used to grow MgO on GaAs using pure Mg metal as the target material in the presence of a high-purity gas having the composition of O_2-Ar, 1–7.5% O_2 at a total pressure of 5×10^{-3} Torr [13]. Nashimoto et al. applied laser ablation for the deposition of MgO using Mg target and the film quality was very sensitive to the amount of the oxygen present in the system[10]. In our study, we evaporated Mg using an effusion cell in the presence O_2 to grow MgO films on GaAs (100). One advantage of this method is that Mg evaporates at lower temperature than that required for the evaporation of MgO. Although in this case, a high oxygen flux (~ 10^{-6} Torr) is required to avoid the desorption of Mg atoms from the substrate. [14] This is in contrast to the direct deposition of MgO where a beam of MgO molecules can be obtained by electron beam evaporation and MgO films can be grown at lower pressures.[14] It is important to note that gas phase $(MgO)_n$ clusters do form and each would have different sticking coefficient on the substrate depending on its structure as well as the number of formula units, *n*.

One of the main issues affecting epitaxial growth of MgO on GaAs (100) is the quality of the GaAs (100) surface prior to MgO deposition. The presence of surface impurities, roughness, and a layer of oxide can strongly affect both epitaxy and interface properties. Therefore, in some of the studies mentioned above, first GaAs films were prepared in situ and then MgO was deposited [1, 4, 7, 8, 15, 16]. In other studies, commercially polished GaAs(100) wafers were used after cleaning by wet chemical methods [3, 5, 9, 10, 14, 17]. In addition, oxide desorption by annealing at higher temperatures in the absence of As flux was used previously for cleaning the GaAs surface [18]. However, often these wet

chemical and annealing methods failed to achieve clean atomically smooth GaAs surfaces and oxide removal was only partial. The best results were achieved by preparing a GaAs (100) layer in situ using standard molecular beam epitaxy (MBE) [19-21]. In our study, GaAs (100) substrate was cleaned and prepared for the growth of MgO by Ar ion sputtering and annealing without using chemical etching or wet chemical methods.

In addition to unique electronic properties of MgO/GaAs systems, MgO can be used as a light penetrating film due to its high band gap. MgO films, which are thicker than 3 nm, have the bulk MgO band gap of 7.83 eV [16]. Therefore, MgO allows passing the whole range of solar radiation hence it may be able to use as a light penetrating protective layer for photo catalysts to avoid photo corrosion in processes associated with solutions or electrolytes such as photo catalytic water splitting and photo oxidation of organics. In order to use MgO as a protective interlayer to separate the surfaces of photo catalysts from solutions or electrolytes to avoid photo corrosion, MgO layer must be stable under reaction conditions. In addition, MgO films must be capable of transferring charge carriers efficiently from semiconductor photo catalysts to the surface of MgO where photo catalytic reactions take place.

Here we report the growth of MgO films on GaAs (100) by evaporating Mg in the presence of oxygen. The grown MgO films were characterized with different techniques including in situ Auger electron spectroscopy (AES), and ex-situ scanning electron microscopy (SEM), X-ray diffraction (XRD), high-resolution transmission electron microscopy (HRTEM), and energy–dispersive X–ray spectroscopy (EDX)). To study the stability of MgO films under aqueous conditions, we investigated the reaction of MgO films with water and with 0.1 M NaOH.

2. Experimental

MgO films on GaAs (100) were grown in a molecular beam epitaxy (MBE) chamber with a base pressure of $\approx 3.0 \times 10^{-10}$ Torr. An effusion cell (CreaTec Fischer & Co.) was used for Mg evaporation. The MBE system is also equipped with Auger Electron Spectroscopy (AES – STAIB, ESA 100), mass spectrometry (SRS, RGA 200), and Ar ion sputtering (Ion Source IQE 11/35, SPECS). The Zn-doped (carrier concentration $=1.17\times10^{19}$- 2.18×10^{19} cm^{-3}; the total numbers of atoms in 1 cm^3 of GaAs is 4.42×10^{22} so the doping is ca. 0.02 – 0.05%) GaAs (100) single crystal wafer (AXT, Inc.) was used to grow MgO films. The temperature of the sample stage was measured by a type-K thermocouple attached to it and the temperature of the GaAs (100) substrate was estimated using a previous temperature calibration performed for the Ti-film/Si (100) substrate by measuring its temperature with a pyrometer. The GaAs(100) (1 cm x 1 cm) substrate was cleaned by Ar ion sputtering (600 V, $\approx 2 \times 10^{-5}$ Torr of Ar) for

~ 30 min at 500 °C and subsequent annealing at 550 °C for one hour. The purity of the substrate was determined by the AES. MgO films on GaAs (100) were grown by evaporation of Mg with the effusion cell (the effusion cell temperature was set at 240 °C). The substrate was first heated to 450 ˚C in vacuum, then the shutter of the Mg doser was opened, next the substrate was turned towards the Mg doser and finally O_2 was introduced into the chamber (5×10^{-6} Torr). The thickness of the film was dictated by the deposition time under a constant Mg flux and approximately 20 nm film was grown after a three-hour deposition.

XRD data were collected with D8 ADVANCE (Bruker) X-ray diffractometer and SEM micrographs were obtained with Verios G4 Scanning Electron Microscope (Thermo Scientific). The cross-sectional MgO/GaAs (100) lamella was prepared using Focused Ion Beam (FIB) technique for HRTEM analysis. Prior to ion-beam milling, MgO deposited GaAs (100) wafer was attached to an Al pin stub using strips of Cu tape. Approximately 10 nm layer of Ir was deposited using Q150T Plus turbomolecular pumped sputter coater to avoid charging during the FIB milling process. First, approximately 25-50 nm amorphous carbon layer was deposited on the area of interest using an electron beam (3 kV, 2.7 nA). Then approximately a 450-500 nm Pt layer was deposited first using the electron beam (3 kV, 2.7 nA) followed by further Pt deposition using an ion beam (30 kV, 0.28 nA). Due to observable damage to the MgO film at typical beam energy values used for preparing lamellae of Si wafer, much lower beam energies were used to avoid any possible damage to the MgO thin film during milling and thinning processes. Typically, the lamella preparation process took about 4-5 hours. Finally, a very thin (≈ 100 nm) lamella was prepared for HRTEM, STEM, and EDX measurements. HRTEM analysis was performed with Titan ST transmission electron microscope equipped with a field emission electron source, which was operated at 300 kV. The microscope was operated in either HRTEM (phase contrast) or HAADF-STEM mode (Z-contrast). The point-to-point resolution was 0.12 nm and the information limit was 0.10 nm. HRTEM beam focus was 100 nm whereas that of STEM was 1.0 nm. EDX analysis was carried out in STEM mode of operation. A double tilt sample holder was used to align the lamella on MgO, GaAs, and MgO/GaAs interface zone axes.

3. Results and Discussion

3.1. Preparation and characterization of MgO films

3.1.1. Auger electron spectroscopy (AES) data

Figure 1 presents Auger Electron Spectra before and after deposition of an MgO film on GaAs (100) with the following procedure. First, the GaAs (100) substrate was cleaned by Ar ion sputtering at

500 °C for 30 minutes and subsequent annealing at 550 °C for one hour. Then AES lines of the cleaned GaAs (100) substrate was obtained as shown by the black spectrum. Before cleaning the GaAs (100) substrate, C, Ca, and O were seen; all were removed after the cleaning process. The MgO film was grown at 450 °C substrate temperature by evaporating Mg under 5.0 x 10^{-6} Torr of O_2 for three hours. The Mg effusion cell temperature was kept at 240 °C. After deposition of MgO, the peaks for Ga and As were not detected as shown by the red spectrum where only AES peaks for Mg and O were present. The peak-to-peak height ratio of Mg(KLL)/O(KLL) after incorporating the AES sensitivity factors [O (KLL) - 0.50 and Mg (KLL) - 0.11] is ≈ 1.0 (Mg:O ≈ 1.0 :1.0). These results indicate that a continuous MgO film is grown on GaAs(100) and it is thick enough so that peaks for the underneath substrate GaAs(100) are not detected (95% of the signal originated from 3 λ ≈ 9 nm) where λ (nm) ≈ 3 nm [22],[23] for the $KE_{As(LMM)}$ = 1258 eV). Considering a d_{MgO} spacing of 0.21 nm (half of the MgO lattice constant) we estimated λ =1.5 nm; using the equation $\lambda\ (nm) = 0.41 \times d^{1.5}_{MgO} \times KE^{0.5}_{GaAs(LMM)}$[24, 25].

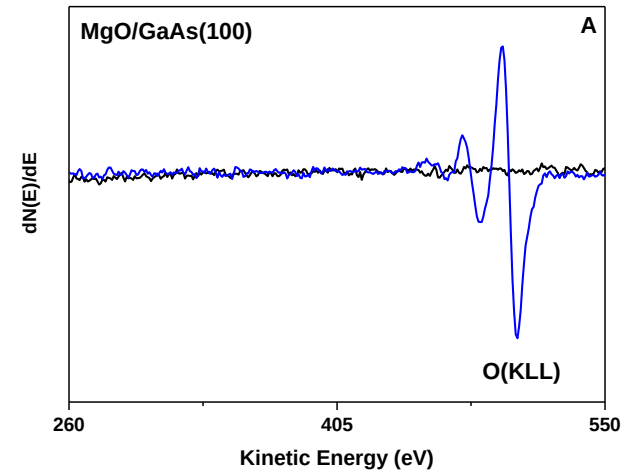

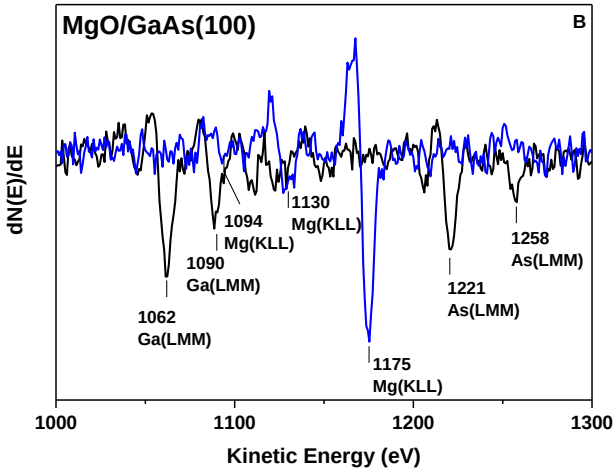

Figure 1.

Auger electron spectra before (black) and after (blue) deposition of an MgO film on GaAs (100) at the following experimental conditions. The GaAs (100) substrate was cleaned by Ar ion sputtering at 500 °C for 30 minutes and subsequent annealing at 550 °C for one hour. The MgO film was grown at 450 °C-substrate temperature by evaporating Mg under 5.0 x 10^{-6} Torr of O_2 for three hours. The Mg cell temperature was kept at 240 °C. A) The dN(E)/dE AES O KLL region before and after deposition. B) The dN(E)/dE AES Mg KLL, Ga LMM and As LMM regions before and after deposition.

3.1.2. X-ray diffraction (XRD) data

Figure 2 presents an XRD spectrum of MgO/GaAs (100) where the MgO film was grown at 450 °C. The XRD spectrum exhibits an MgO (200) peak for the MgO film and GaAs substrate peaks, (200) and (400), indicating that the MgO film has grown predominantly in the cubic phase with the (100) plane parallel to the substrate. Two possible heteroepitaxial relationships between GaAs (100) and MgO planes, MgO [110]‖GaAs [100] and MgO [100] ‖GaAs [100], have been reported [3]. The lattice constants of GaAs and MgO are 5.6538 and 4.213 Å, respectively[3].

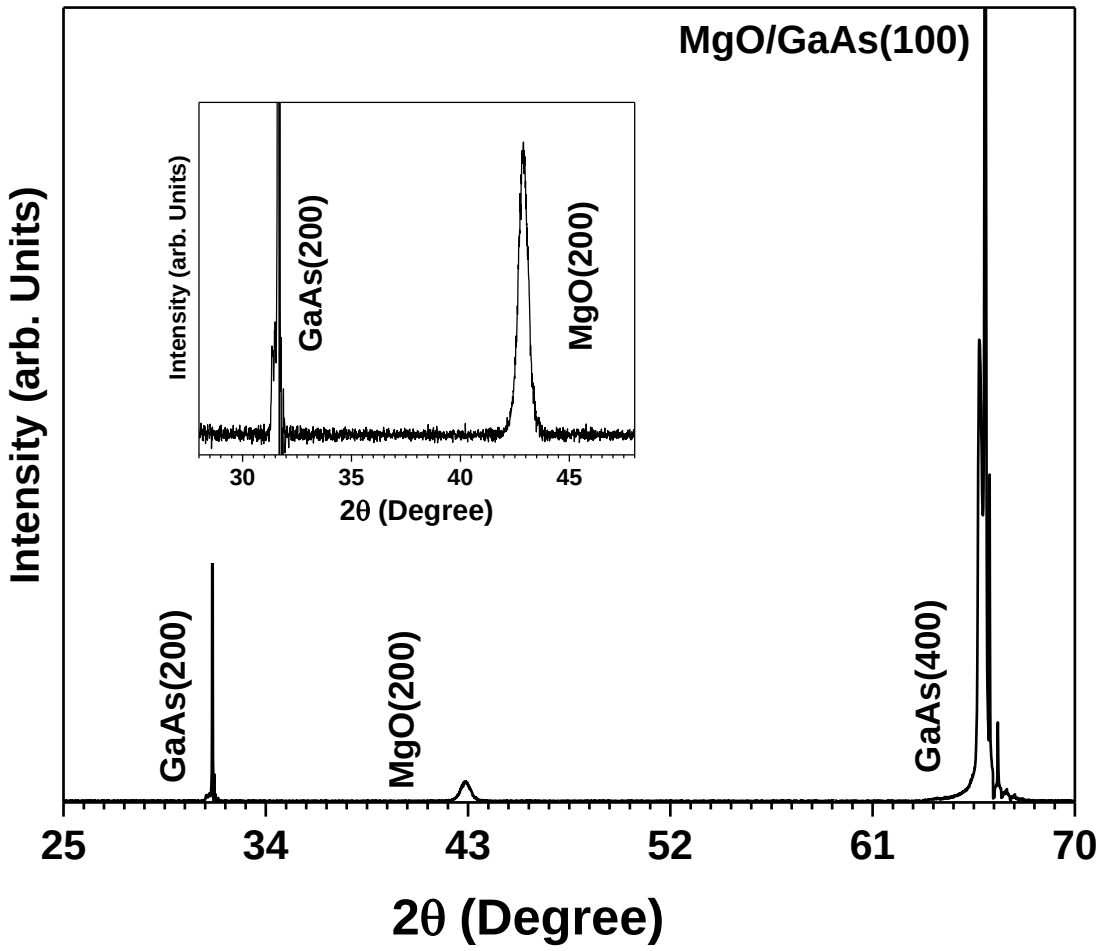

Figure 2.

X-ray diffraction pattern of an MgO film grown on GaAs (100) at 450 °C. The inset is a magnifying region of the GaAs (200) and MgO (200) diffraction patterns.

The lattice misfit [(a_{GaAs} - a_{MgO})/a_{MgO}][1] of heteroepitaxial relationship between MgO[100] ‖ GaAs[100] is 34.2% whereas it is 5.1% for MgO [110]‖GaAs[100] heteroepitaxial relationship. Despite the higher misfit, the XRD data shows that MgO (100) is grown on GaAs (100). However, in order to see the growth configuration and to see whether it is epitaxial growth, analysis by other techniques such as TEM and reflection high-energy electron diffraction (RHEED) is required. The HRTEM analysis of MgO/GaAs (100) are shown in section 3.1.4.

In the XRD spectrum, the position of MgO(200) peak is at 42.9°, which is very close to values reported for a MgO film grown on GaAs(100) and bulk MgO crystals at 42.92° and 42.89°, respectively [3]. These XRD results suggest that the MgO film grown on GaAs (100) has bulk properties. The full width at half maximum (FWHM) of the MgO(200) peak is 0.52 , which is similar to the FWHM of 0.6 reported previously for a MgO(100) film grown on GaAs(100) at 200 °C[1]. In general, the FWHM decreases with increasing growth temperature due to better crystalline ordering of films. The MgO films on GaAs(100) grown at 250, 300, 350, 400, and 450 °C temperatures had FWHM (XRD) peaks equal 0.70, 0.70, 0.70, 0.52, and 0.52°, respectively.

3.1.3. Scanning electron microscopy (SEM) data

The SEM micrographs of MgO films grown on GaAs (100) at 450 °C are shown in Figure 3. The SEM micrograph obtained immediately after preparing the MgO film is presented in Figure 3A, where a nearly featureless structure is seen with no signs of granular crystallites indicating that the film grown at 450 °C is smooth. The SEM micrograph in Figure 3B was obtained after exposing the MgO film to air for ≈ six hours, some white regions or spots are seen. MgO when exposed to air reacts with H_2O and CO_2 to form hydroxides, hydrogenocarbonates and carbonates as reported in a previous study [26, 27]. Longer exposure to air led to larger white areas as shown by the SEM micrograph in Figure 3C, obtained after exposing the MgO film to air for 8 days. Based on the EDX analysis, white areas are $Mg(OH)_2$ and the dark regions may be composed of MgO, $Mg(HCO_3)_2$ and $MgCO_3$(supporting information Figure S1). Similar results were obtained after immersing MgO/GaAs(100) in water for 5 hours at room temperature as shown by the SEM micrograph in Figure 3D.

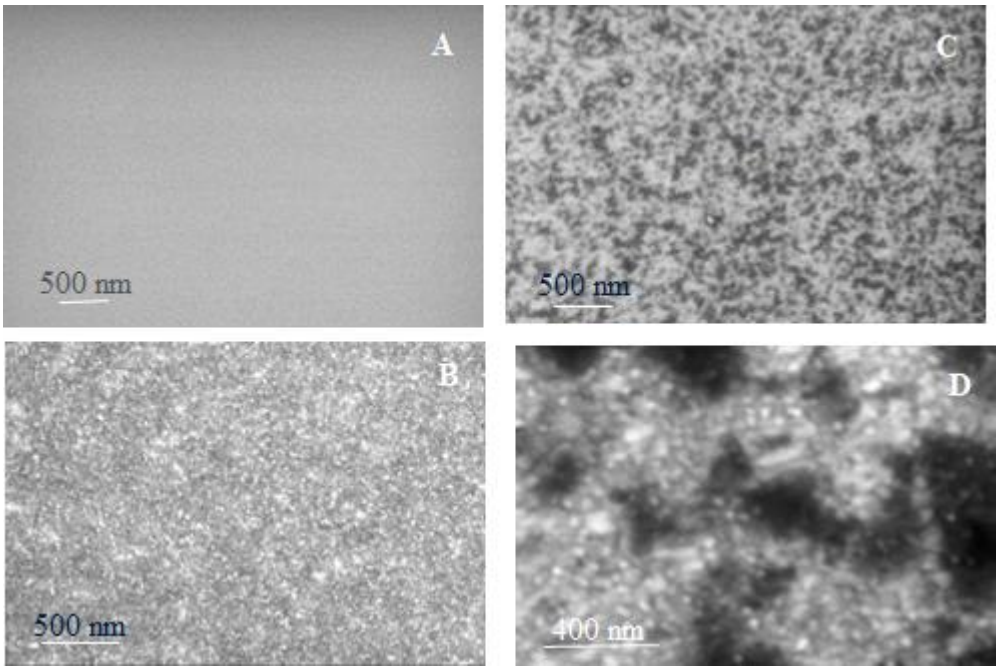

Figure 3.

SEM micrographs of an MgO film grown on GaAs (100) at 450 °C. A) Fresh after preparing the MgO film, exposed to ambient conditions before imaging B) Kept in ambient conditions for ≈ six hours C) Kept in ambient conditions for eight days. D) After immersing MgO/GaAs (100) in water for five hours.

3.1.4. Ttransmission electron microscopy (TEM) and energy–dispersive X–ray spectroscopy (EDX) data

To see whether the MgO film was grown epitaxially on GaAs (100), cross sectional HRTEM micrographs of an MgO/GaAs (100) lamella prepared by FIB milling were obtained. Figure 4A presents the TEM micrograph of an MgO/GaAs (100) lamella with Ir, C, and Pt layers deposited on top of the MgO film. The thickness of the MgO layer is 19 nm whereas the thicknesses of the deposited Ir and C layers on top of MgO film are ≈10 nm, and ≈35 nm, respectively. Pt layer is present on top of the C layer. Chemical identities of MgO and GaAs layers were confirmed by EDX in STEM mode of operation as shown in Figure 4B. Spectrum 1 obtained from region 1 shows peaks for Mg and O confirming the presence of MgO. In addition, spectrum 1 presents a peak for Cu that comes from the Cu TEM grid. A peak for C is also present in both spectra. Spectrum 2 collected from region 2 shows peaks for As and Ga as expected. The FFT images shown in Figures 4C and 4D for MgO and GaAs, respectively, indicate that they are single crystalline. The insets in Figures 4C and 4D, which present TEM micrographs of MgO and GaAs regions, respectively, further confirm that GaAs and MgO are single crystalline.

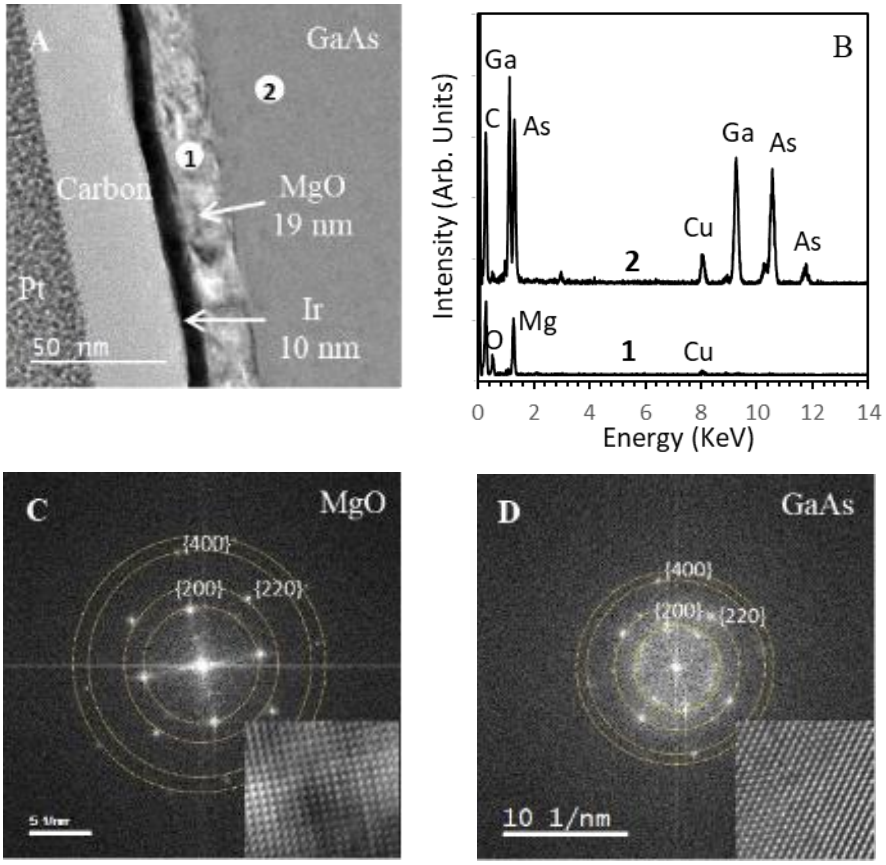

Figure 4.

A) A cross sectional TEM micrograph of MgO/GaAs (100) lamella prepared by FIB milling. Prior to ion-beam milling, layers of Ir (≈10 nm), C (≈35 nm) and Pt (≈500 nm) were deposited on top of the MgO film to preserve the surface from damage by high energy Ga^+ ion beam used for the milling process. B) EDX spectra obtained from the regions 1 and 2 specified in A. C) and D) FFT images of MgO and GaAs, respectively. Insets present TEM micrographs of MgO and GaAs.

To see the interface between GaAs and MgO, a cross sectional HRTEM micrograph of the MgO/GaAs (100) interface was obtained as shown in Figures 5A and 5B. A clear interface between MgO and GaAs is present and it is not distorted when changing from GaAs to MgO lattice. The electron beam is oriented along the GaAs [001] direction and the TEM micrograph shows that the MgO film has grown in the cubic phase with the (100) plane parallel to GaAs (100). The insets in Figure 5A present FFT images for MgO and GaAs obtained from the areas in close proximity to the interface. The FFT images were obtained by keeping one side of the squared ROI (region of interest) in Gatan software on the broken line. The broken line indicates the interface between GaAs and MgO and connects the

meeting points of the straight lines drawn along the lattice planes of both materials (MgO followed by GaAs). These FFT images indicate that MgO and GaAs located close to the interface are single crystalline as they are exactly the same as the FFT images obtained from MgO and GaAs regions away from the interface as shown in Figures 4C and 4D, respectively. This also indicates the absence of any significant surface oxidation of GaAs as distortion in FFT due to the presence of Ga_2O_3 or As_2O_3/As_2O_5 was not observed. It is to be noted that Ga_2O_3 has trigonal, monoclinic and hexagonal as its most commonly found crystal structures [28]. As_2O_3 has monoclinic as well as cubic crystal structures [29] while As_2O_5 has . orthorhombic and tetragonal crystal structures [30]. The lattice parameters of both oxides differ from the one obtained and therefore their formation can be ruled out [31],[32]. Since HRTEM shows a reconstruction starting from the second layer, and since above this layer the diffraction pattern is that of MgO, then the interface may be composed of Ga-O-Mg and As-O-Mg bonds.

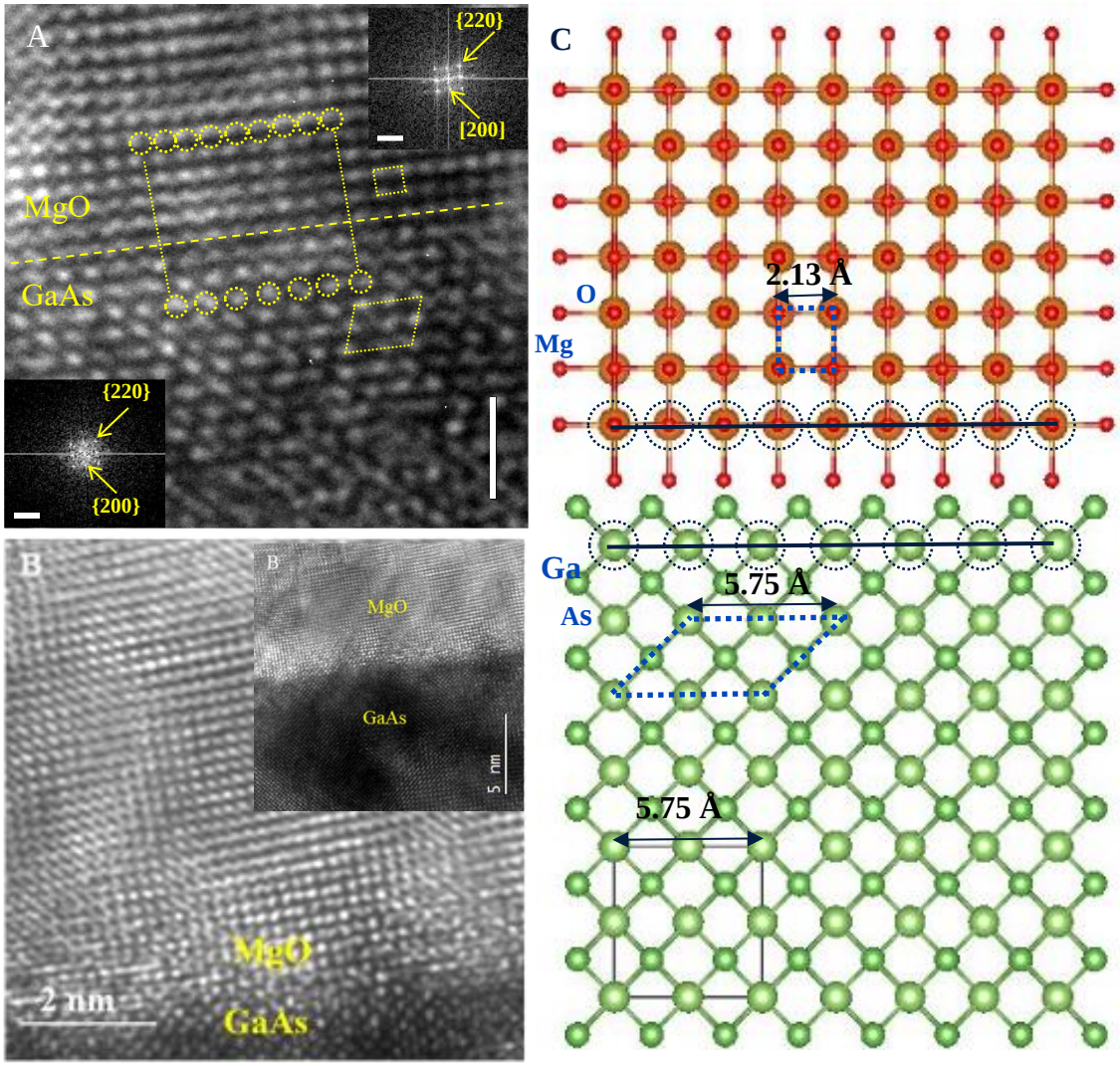

Figure 5.

A) and B) cross sectional HRTEM micrographs of MgO/GaAs (100), the inset in B is a larger area of the film. C) A model structure constructed in such a way that MgO (100) plane is parallel to GaAs (100). The square and parallelogram shown by blue dotted lines on MgO and GaAs in the model structure, respectively, correspond to those marked in yellow dotted lines on the TEM micrograph A. The 4 : 3 superstructure consisting of 4 MgO (100) unit cells on top of 3 GaAs (100) unit cells is shown by the yellow dotted circles drawn in TEM micrograph A. In the model structure, dotted circles and black lines drawn show the 4:3 relationship

The MgO/GaAs model structure shown in Figure 5C is constructed in such a way that MgO (100) and GaAs (100) planes are parallel and this model structure helps to interpret the epitaxial growth of MgO (100) on top of GaAs (100). The square and parallelogram shown by blue dotted lines on MgO and GaAs, respectively, in the model structure, correspond to those marked in yellow dotted lines on the TEM micrograph in Figure 5A. In addition, distances between adjacent (100) planes (d space) in MgO and GaAs in the model structure are the same as those in the TEM micrograph. The XRD peak for MgO (200) at 42.1° in Figure 2 corresponds to the d spacing in the TEM micrograph of MgO. Both TEM and XRD results clearly indicate the presence of MgO [100] ‖ GaAs [100], heteroepitaxial relationship in spite of 34.2% of lattice misfit. Despite the higher misfit, the epitaxial MgO(100) is grown on GaAs(100) due to the 4 : 3 relationship (4 aMgO : 3 aGaAs) between MgO(100) and GaAs(100)[1]. The formation of a 4:3 superstructure reduces the lateral misfit between MgO (100) and GaAs (100) to ≈0.65%. The 4:3 superstructure consisting of 4 MgO(100) unit cells on top of 3 GaAs(100) unit cells is shown by the yellow dotted circles drawn, which evidences the epitaxial growth with MgO(100)[001] ‖ GaAs(100)[001]. In the model structure, the dotted circles and the black lines drawn show the 4:3 relationship. These results confirm the epitaxial growth of MgO (100) on top of GaAs (100). The ordered MgO layer is continued from the interface towards the film surface as shown by Figure 5B. The epitaxial growth of MgO also indicates that the preparation of GaAs (100) substrate by Ar sputtering and subsequent annealing provides a clean and flat surface for the growth of epitaxial MgO (100) layer on top of GaAs (100)

3.2. Reaction of MgO films with NaOH

3.2.1 Scanning electron microscopy (SEM) data

To investigate the reaction of MgO film with NaOH, the MgO (100)/GaAs (100) sample was immersed inside a solution of 0.1 M NaOH for five hours at room temperature and SEM micrographs were collected as shown in Figure 6. NaOH was chosen as a typical alkaline medium where the water splitting reaction would occur using an alkaline membrane[33]). The plan view of the SEM micrograph in Figure 6A shows flake-like structures, with some protrusions in certain areas as shown by the 35°-tilt view of SEM micrograph in Figure 6B. The EDX data (not shown) obtained from white protruding regions show more O relative to dark areas suggesting that white protrusions are $Mg(OH)_2$. These SEM micrographs show that $Mg(OH)_2$ structures develop into a continuous porous network. Similar flake-like structures were reported for $Mg(OH)_2$ formed on a Mg film after it was immersed in a saturated $Mg(OH)_2$ solution[34]. The SEM micrograph in Figure 6B shows that flake-like $Mg(OH)_2$ structures are formed on top of MgO and this is further confirmed by TEM micrographs shown below.

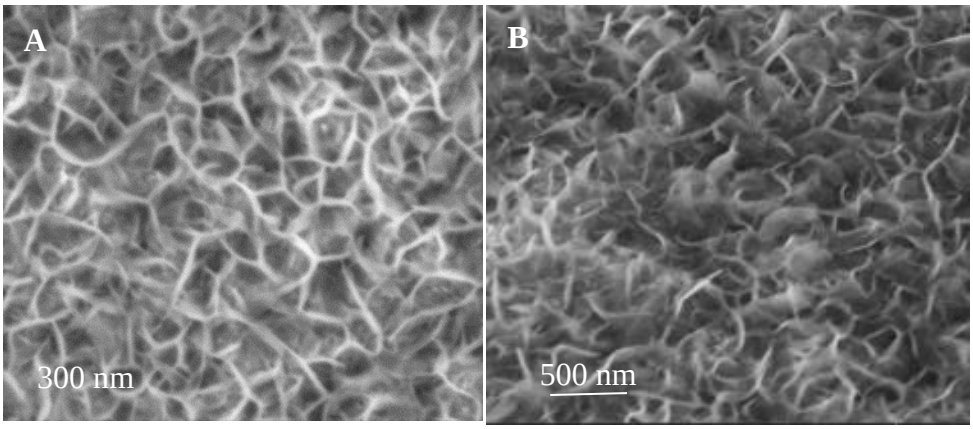

Figure 6.
SEM micrographs obtained after immersing MgO/GaAs (100) inside a solution of 0.1 M NaOH for five hours. A) Plan view and B) 35°-tilt view. The MgO film was grown on GaAs (100) at 450 °C.

3.2.2. Transmission electron microscopy (TEM) and energy–dispersive X–ray spectroscopy (EDX) data

To see the morphology and the interface between $Mg(OH)_2$ and MgO after immersing MgO (100)/GaAs (100) in a solution of 0.1 M NaOH for five hours, TEM analysis was carried out. Figures 7A and 7B present cross sectional TEM micrographs and Figure 7C presents EDX spectra for the regions specified in Figure 7A. The EDX spectrum collected from GaAs, region 1, shows peaks only for As and Ga as expected. The presence of MgO is shown by the EDX spectrum taken from region 2. The EDX

spectrum collected form region 3 shows peaks for Mg and Pt, which was deposited prior to ion-beam milling during the preparation of the lamella for TEM analysis. This data shows that the presence of Pt in between $Mg(OH)_2$ protrusions. Less intense peaks for Mg and O and an intense peak for Pt are shown by the spectrum collected from region 4 indicating the possible presence of $Mg(OH)_2$ away from the MgO layer. Mg is not present in region 5 but peaks for Pt and Ga are present. Cu shown in EDX spectra originates from Cu TEM grid.

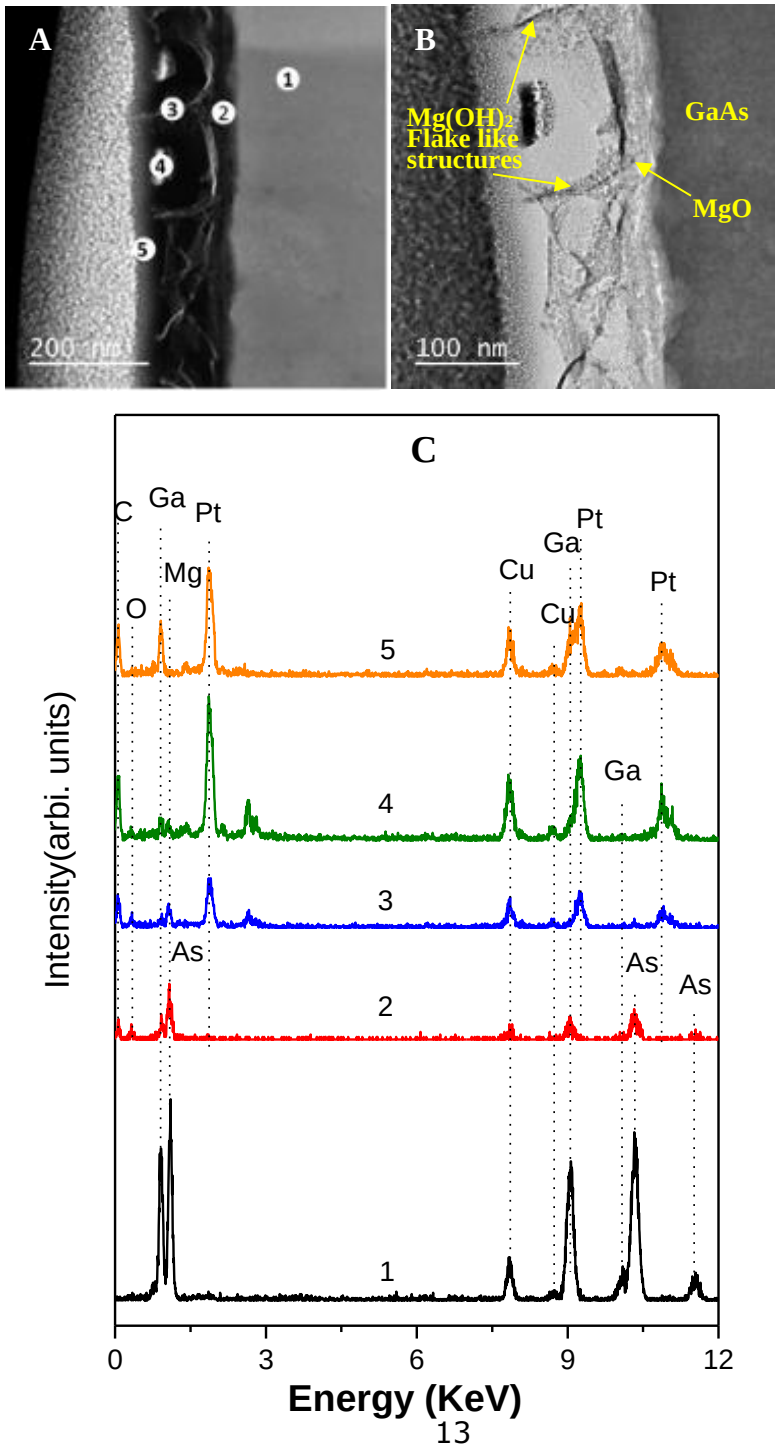

Figure 7.

A) and B) cross sectional TEM micrographs obtained after immersing MgO/GaAs (100) inside a solution of 0.1 M NaOH for five hours. C) EDX spectra for the specified regions in Figure 7A.

Figure 7B may indicate flake-like $Mg(OH)_2$ structures formed on the MgO film after it reacts with NaOH. The sub-surface MgO is dense, whereas the surface has less dense and flake-like $Mg(OH)_2$ structures. These flake-like $Mg(OH)_2$ structures are also identified as possible structures in the SEM images shown in Figure 6. The TEM micrographs further show that these protrusions grow up to 25 nm above the MgO surface, which is also confirmed by the EDX data in Figure 7C. Similar growth of $Mg(OH)_2$ on Mg surface was observed previously [34]. These results indicate that within the experimental conditions NaOH reacts with MgO to form $Mg(OH)_2$ at some depth while still the underneath MgO layer stayed in contact with the GaAs substrate.

As mentioned in the introduction section, the wide band gap MgO allows passing the whole range of solar radiation. However, to use MgO films as a light penetrating protective layer for photo catalysts to avoid photo corrosion, the MgO film must be stable and able to transfer charge carriers from the semiconductor to the surface of MgO. One of the main factors that determines the charge carrier transfer is the band alignments at the interface. Figure 8 shows a schematic band alignment diagram for interfaces of MgO/GaAs and MgO/$GaInP_2$ as well as MgO defect states derived from previously reported data for MgO/GaAs [16], $GaInP_2$/GaAs [35], and MgO [36]. Based on band alignments of the GaAs and MgO interface, electrons cannot be transferred from GaAs to the MgO conduction band [16].

Solar cells are used in photo electro chemical (PEC) water splitting but they are prone to photo-corrosion immediately after contacting with solutions or electrolytes. Therefore, there is a need for protective interlayer between the solar cell surface and electrolytes [37, 38]. To use MgO as a protection layer for solar cells with a top layer of $GaInP_2$, MgO must be stable under reaction conditions and it must be able to transfer electrons efficiently (from $GaInP_2$ to MgO film). This depends on the band alignments of the interface of $GaInP_2$ and MgO. Based on the band alignments of the interface of $GaInP_2$ and MgO shown in Figure 8, any possible electron injection from semiconductor surfaces to MgO would occur via defects or electron tunneling. The latter strongly depends on the thickness of the MgO layer and in general tunneling occurs only with oxide layers of thickness less than ≈2-3 nm. In MgO, various defect centers such as oxygen vacancies (F-center defects), Mg vacancies (V- center defects), neutral Mg + neutral O vacancies (P center, Schottky defects), and interstitial oxygen etc…co-exist [36]. Some of

these defect states reported previously are included in the schematic band alignment diagram shown in Figure 8[36]. Based on the band positions of MgO defect states, electrons from GaAs and $GaInP_2$ can be injected to MgO films through defect states if they are present in the epitaxial MgO films. However, in order to use MgO as a protection layer, the stability of the MgO film under reaction conditions in the presence of photoreactions also needs to be considered. The reaction of MgO films with NaOH leads to form flake-like $Mg(OH)_2$ structures at the upper layers while the underneath seems to indicate that MgO is still in contact with GaAs. Considering both stability of MgO under alkaline conditions and electron transferability from semiconductor surfaces to MgO through defect states, the MgO films can be considered for further studies as a protection layer for photo catalysts in photo electrochemical processes.

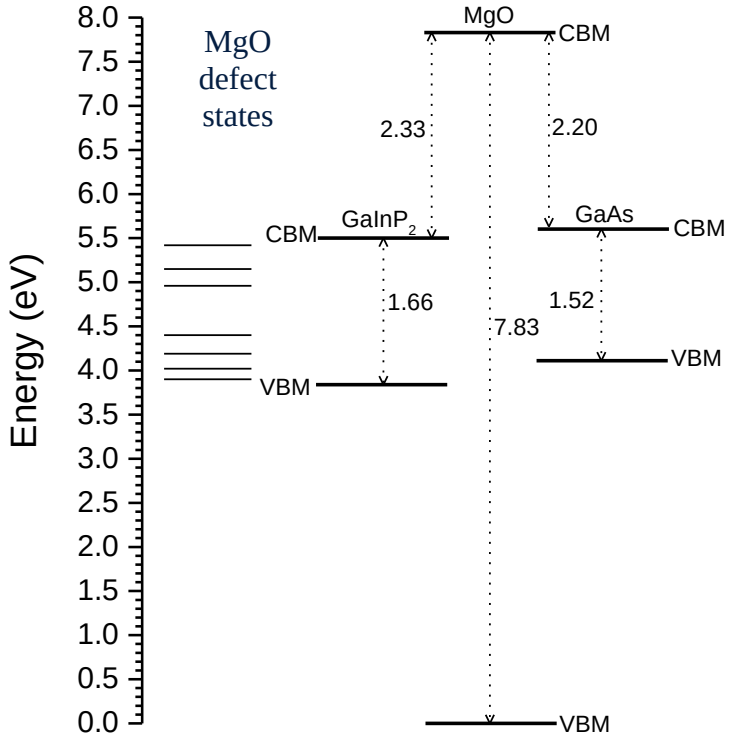

Figure 8.

Schematic band alignment diagram for interfaces of MgO/GaAs and $MgO/GaInP_2$ as well as MgO defect states derived from previously reported data for MgO/GaAs [16], $GaInP_2$/GaAs [35], and MgO [36]. All energies are in eV.

4. Conclusions

The preparation procedure of the GaAs (100) substrate by Ar ion sputtering and subsequent annealing without any wet chemical methods provides a clean and smooth surface for the growth of epitaxial MgO films. AES results show that stoichiometric MgO is grown without other impurities within the detection limit of the spectrometer. XRD results show that better crystalline order can be achieved at the growth temperature in the range of 400-450 °C. Further, XRD patterns indicate that the MgO film has grown predominantly in the cubic phase with the (100) plane parallel to the GaAs (100) substrate. HRTEM results have confirmed the epitaxial growth of MgO on GaAs (100) with MgO (100)[001]‖GaAs (100)[001]. Despite the higher misfit, the epitaxial MgO (100) is grown on GaAs (100) due to the 4 : 3 relationship (4 aMgO : 3 aGaAs) between MgO (100) and GaAs (100). The formation of a 4:3 superstructure reduces the lateral misfit between MgO (100) and GaAs (100) to ≈0.65%. When MgO film is exposed to air, it reacts with H_2O and CO_2 to form hydroxides and carbonates, respectively, on the top layers of the MgO film. The reaction of MgO film with NaOH leads to flake-like structures with some protrusions, which develop into a continuous porous network. These flake-like structures are attributed to $Mg(OH)_2$ and appear to be present only on the surface and near surface while still the underneath was composed of MgO layer, in contact with the GaAs substrate.

5. References

[1] S.B. Wang, A. Sarkar, M. Gruber, R. Koch, Epitaxy and stress of MgO/GaAs(001) heterostructures, J. Appl. Phys., 114 (2013) 154511.

[2] A. Masuda, K. Nashimoto, Orientation of MgO Thin Films on Si(100) and GaAs(100) Prepared by Electron-Beam Evaporation, Japanese Journal of Applied Physics, 33 (1994) L793-L796.

[3] W.Y. Hsu, R. Raj, MgO epitaxial thin-films on (100) GaAs as a substrate for the growth of oriented $PbTiO_3$, Applied Physics Letters, 60 (1992) 3105-3107.

[4] X. Jiang, R. Wang, R.M. Shelby, R.M. Macfarlane, S.R. Bank, J.S. Harris, S.S.P. Parkin, Highly spin-polarized room-temperature tunnel injector for semiconductor spintronics using MgO(100), Phys. Rev. Lett., 94 (2005) 056601.

[5] S. Chromik, M. Spankova, I. Vavra, J. Liday, P. Vogrincic, P. Lobotka, Preparation and structural properties of MgO films grown on GaAs substrate, Applied Surface Science, 254 (2008) 3635-3637.

[6] T.W. Kim, Y.S. You, Microstructural and electrical properties of MgO thin films grown on p-GaAs (100) substrates, Mater. Res. Bull., 36 (2001) 747-754.

[7] A. Sarkar, S.B. Wang, W. Grafeneder, M. Arndt, R. Koch, Ultrathin MgO diffusion barriers for ferromagnetic electrodes on GaAs(001), Nanotechnology, 26 (2015) 165203.
[8] Y. Lu, J.C. Le Breton, P. Turban, B. Lépine, P. Schieffer, G. Jézéquel, Measurement of the valence-band offset at the epitaxial MgO-GaAs(001) heterojunction by x-ray photoelectron spectroscopy, Applied Physics Letters, 88 (2006) 042108.
[9] W. Prusseit, S. Corsépius, F. Baudenbacher, K. Hirata, P. Berberich, H. Kinder, Epitaxial growth of $YBa_2Cu_3O_7$ films on GaAs with MgO buffer layers, Applied Physics Letters, 61 (1992) 1841-1843.
[10] K. Nashimoto, D.K. Fork, T.H. Geballe, Epitaxial-growth of MgO on GaAs(001) for growing epitaxial $BaTiO_3$ thin-films by pulsed laser deposition, Applied Physics Letters, 60 (1992) 1199-1201.
[11] D.K. Fork, K. Nashimoto, T.H. Geballe, Epitaxial $YBa_2Cu_3O_7$-δ on GaAs(001) using buffer layers, Applied Physics Letters, 60 (1992) 1621-1623.
[12] J. Bruley, S. Stemmer, F. Ernst, M. Rühle, W.-Y. Hsu, R. Raj, Nanostructure and chemistry of a (100)MgO/(100) GaAs interface, Applied Physics Letters, 65 (1994) 564-566.
[13] R. Soto, S. Mergui, P.E. Schmidt, Electrical and mechanical properties of MgO thin films on GaAs, Thin Solid Films, 308-309 (1997) 611-614.
[14] L.S. Hung, L.R. Zheng, T.N. Blanton, Epitaxial growth of MgO on (100)GaAs using ultrahigh vacuum electron-beam evaporation, Applied Physics Letters, 60 (1992) 3129-3131.
[15] Y. Li, Y. Chye, Y.F. Chiang, K. Pi, W.H. Wang, J.M. Stephens, S. Mack, D.D. Awschalom, R.K. Kawakami, Inversion of Ferromagnetic Proximity Polarization by MgO Interlayers, Phys. Rev. Lett., 100 (2008) 237205.
[16] Y. Lu, J.C. Le Breton, P. Turban, B. Lepine, P. Schieffer, G. Jezequel, Measurement of the valence-band offset at the epitaxial MgO-GaAs(001) heterojunction by x-ray photoelectron spectroscopy, Applied Physics Letters, 88 (2006) 042108
[17] M.Z. Tseng, C. Nguyen, E. Tarsa, L.D. Chang, E.L. Hu, H. Kroemer, Temperature-dependent mobility of a GaAs/AlGaAs heterostructure after deposition of MgO and superconducting $YBa_2Cu_3O_{7-x}$, Applied Physics Letters, 61 (1992) 601-603.
[18] C.T. Foxon, J.A. Harvey, B.A. Joyce, The evaporation of GaAs under equilibrium and non-equilibrium conditions using a modulated beam technique, Journal of Physics and Chemistry of Solids, 34 (1973) 1693-1701.
[19] C. Xu, J.S. Burnham, R.M. Braun, S.H. Goss, N. Winograd, Tilting in the arsenic-induced c(4×4) reconstruction of the GaAs{001} surface, Physical Review B, 52 (1995) 5172-5178.

[20] J. Herfort, H.-P. Schönherr, B. Jenichen, Magnetic and structural properties of ultrathin epitaxial Fe3Si films on GaAs(001), J. Appl. Phys., 103 (2008) 07B506.
[21] B.D. Schultz, C. Adelmann, X.Y. Dong, S. McKernan, C.J. Palmstrøm, Phase formation in the thin film Fe/GaAs system, Applied Physics Letters, 92 (2008) 091914.
[22] S. Tanuma, C.J. Powell, D.R. Penn, Calculations of electorn inelastic mean free paths. II. Data for 27 elements over the 50–2000 eV range, Surface and Interface Analysis, 17 (1991) 911-926.
[23] J.N. Wilson, R.M. Dowler, H. Idriss, Adsorption and reaction of glycine on the rutile TiO_2(011) single crystal surface, Surface Science, 605 (2011) 206-213.
[24] G. Ertl;, J. Kuppers;, Low Energy Electrons and Surface Chemistry 2nd Edition ed., Wiley-VCH, Weinheim, Federal Republic of Germany, 1986.
[25] M.P. Seah, W.A. Dench, Quantitative electron spectroscopy of surfaces: A standard data base for electron inelastic mean free paths in solids, Surface and Interface Analysis, 1 (1979) 2-11.
[26] P. Casey, E. O'Connor, R. Long, B. Brennan, S.A. Krasnikov, D. O'Connell, P.K. Hurley, G. Hughes, Growth, ambient stability and electrical characterisation of MgO thin films on silicon surfaces, Microelectron. Eng., 86 (2009) 1711-1714.
[27] D.K. Aswal, K.P. Muthe, S. Tawde, S. Chodhury, N. Bagkar, A. Singh, S.K. Gupta, J.V. Yakhmi, XPS and AFM investigations of annealing induced surface modifications of MgO single crystals, Journal of Crystal Growth, 236 (2002) 661-666.
[28] Y. Yao, S. Okur, L.A. Lyle, G.S. Tompa, T. Salagaj, N. Sbrockey, R.F. Davis, L.M. Porter, Growth and characterization of α-, β-, and ϵ-phases of Ga_2O_3 using MOCVD and HVPE techniques, Materials Research Letters, 6 (2018) 268-275.
[29] W.B. Pearson, A handbook of lattice spacings and structures of metals and alloys: International series of monographs on metal physics and physical metallurgy, Elsevier, 2013.
[30] S. Redfern, E. Salje, Spontaneous strain and the ferroelastic phase transition in As_2O_5, Journal of Physics C: Solid State Physics, 21 (1988) 277.
[31] P. Ballirano, A. Maras, Refinement of the crystal structure of arsenolite, As_2O_3, Zeitschrift für Kristallographie-New Crystal Structures, 217 (2002) 177-178.
[32] M. Jansen, Crystal Structure of As2O5, Angewandte Chemie Int. Ed., 16 (177) 314-315.
[33] M.A. Khan, I. Shankiti, A. Ziani, N. Wehbe, H. Idriss, A stable integrated photo-electrochemical reactor for H_2 production from water with STH of 18% at 15 suns and 13% at 207 suns., Angewandte Chemie Submitted, (2020).

[34] S.H. Salleh, S. Thomas, J.A. Yuwono, K. Venkatesan, N. Birbilis, Enhanced hydrogen evolution on Mg $(OH)_2$ covered Mg surfaces, Electrochimica Acta, 161 (2015) 144-152.
[35] S. Froyen, A. Zunger, A. Mascarenhas, Polarization fields and band offsets in GaInP/GaAs and ordered/disordered GaInP superlattices, Applied Physics Letters, 68 (1996) 2852-2854.
[36] N. Pathak, P.S. Ghosh, S.K. Gupta, R.M. Kadam, A. Arya, Defects induced changes in the electronic structures of MgO and their correlation with the optical properties: a special case of electron–hole recombination from the conduction band, RSC Advances, 6 (2016) 96398-96415.
[37] E. Verlage, S. Hu, R. Liu, R.J.R. Jones, K. Sun, C.X. Xiang, N.S. Lewis, H.A. Atwater, A monolithically integrated, intrinsically safe, 10% efficient, solar-driven water-splitting system based on active, stable earth-abundant electrocatalysts in conjunction with tandem III-V light absorbers protected by amorphous TiO2 films, Energy & Environmental Science, 8 (2015) 3166-3172.
[38] L. Kornblum, D.P. Fenning, J. Faucher, J. Hwang, A. Boni, M.G. Han, M.D. Morales-Acosta, Y. Zhu, E.I. Altman, M.L. Lee, C.H. Ahn, F.J. Walker, Y. Shao-Horn, Solar hydrogen production using epitaxial $SrTiO_3$ on a GaAs photovoltaic, Energy & Environmental Science, 10 (2017) 377-382.

Figure Captions

Figure 1. Auger electron spectra before (black) and after (blue) deposition of an MgO film on GaAs (100) at the following experimental conditions. The GaAs (100) substrate was cleaned by Ar ion sputtering at 500 °C for 30 minutes and subsequent annealing at 550 °C for one hour. The MgO film was grown at 450 °C-substrate temperature by evaporating Mg under 5.0×10^{-6} Torr of O_2 for three hours. The Mg cell temperature was kept at 240 °C. A) The dN(E)/dE AES O KLL region before and after deposition. B) The dN(E)/dE AES Mg KLL, Ga LMM and As LMM regions before and after deposition.

Figure 2. X-ray diffraction pattern of an MgO film grown on GaAs (100) at 450 °C. The inset is a magnifying region of the GaAs (200) and MgO (200) diffraction patterns.

Figure 3. SEM micrographs of an MgO film grown on GaAs (100) at 450 °C. A) Right after preparing the MgO film. After exposing the MgO film to air B) for ≈ six hours and C) for 8 days. D) After immersing MgO/GaAs (100) inside water for five hours.

Figure 4. A) A cross sectional TEM micrograph of MgO/GaAs (100) lamella prepared by FIB milling. Prior to ion-beam milling, layers of Ir (≈10 nm), C (≈35 nm) and Pt (≈500 nm) were deposited on top of the MgO film to preserve the surface from damage by high energy Ga^+ ion beam used for the milling process. B) EDX spectra obtained from the regions 1 and 2 specified in A. C) and D) SAED patterns of MgO and GaAs, respectively. Insets present TEM micrographs of MgO and GaAs.

Figure 5. A) And B) cross sectional TEM micrographs of MgO/GaAs (100). C) A model structure constructed in such a way that MgO (100) plane is parallel to GaAs (100). The square and parallelogram shown by blue dotted lines on MgO and GaAs in the model structure, respectively, correspond to those marked in yellow dotted lines on the TEM micrograph A. The 4 : 3 superstructure consisting of 4 MgO (100) unit cells on top of 3 GaAs (100) unit cells is shown by the yellow dotted circles drawn in TEM micrograph A. In the model structure, dotted circles and black lines drawn show the 4:3 relationship.

Figure 6. SEM micrographs obtained after immersing MgO/GaAs (100) inside a solution of 0.1 M NaOH for five hours. A) Plan view and B) 35°-tilt view. The MgO film was grown on GaAs (100) at 450 °C.

Figure 7. A) and B) cross sectional TEM micrographs obtained after immersing MgO/GaAs (100) inside a solution of 0.1 M NaOH for five hours. C) EDX spectra for the specified regions in Figure 7A.

Figure 8. Schematic band alignment diagram for interfaces of MgO/GaAs and MgO/$GaInP_2$ as well as MgO defect states derived from previously reported data for MgO/GaAs [16], $GaInP_2$/GaAs [35], and MgO [36]. All energies are in eV.